Experimental assessment of the influence of welding process parameters on Lamb wave transmission across ultrasonically welded thermoplastic composite joints

Viegas Ochoa de Carvalho, P.A.; Fernandez Villegas, Irene; Groves, Roger M.; Benedictus, Rinze

DOI
10.1016/j.ymssp.2017.06.009

Publication date
2018

Document Version
Final published version

Published in
Mechanical Systems and Signal Processing

Mechanical Systems and Signal Processing 99 (2018) 197–218

Contents lists available at ScienceDirect

Mechanical Systems and Signal Processing

journal homepage: www.elsevier.com/locate/ymssp

Experimental assessment of the influence of welding process parameters on Lamb wave transmission across ultrasonically welded thermoplastic composite joints

Pedro Ochôa [a,b,*], Irene Fernandez Villegas [a], Roger M. Groves [b], Rinze Benedictus [a]

[a] Structural Integrity and Composites Group, Faculty of Aerospace Engineering, TU Delft, Kluyverweg 1, 2629 HS Delft, The Netherlands
[b] Aerospace Non-Destructive Testing Laboratory, Faculty of Aerospace Engineering, TU Delft, Kluyverweg 1, 2629 HS Delft, The Netherlands

ARTICLE INFO

Article history:
Received 18 July 2016
Received in revised form 2 June 2017
Accepted 8 June 2017
Available online 20 June 2017

Keywords:
Thermoplastic composite
Ultrasonic welding
Lamb wave
Structural health monitoring

ABSTRACT

One of the advantages of thermoplastic composites relative to their thermoset counterparts is the possibility of assembling components through welding. Ultrasonic welding in particular is very promising for industrialization. However, uncertainty in the fatigue and fracture behaviour of composites is still an obstacle to the full utilisation of these materials. Health monitoring is then of vital importance, and Lamb wave techniques have been widely recognised as some of the most promising approaches for that end. This paper presents the first experimental study about the influence of welding travel on the transmission of Lamb waves across ultrasonically welded thermoplastic composite joints in single-lap configuration. The main aim of this research is to start to understand how guided waves interact with the internal structure of ultrasonic welds, so that benign, manufacturing-related structural features can be distinguished from damaging ones in signal interpretation. The power transmission coefficient and the correlation coefficient proved to be suitable for analysing the wave propagation phenomena, allowing quantitative identification of small variations of weld-line thickness and intermolecular diffusion at the weld interface. The conclusions are used to develop a tentative damage detection criterion which can later on assist the design of a Lamb wave based structural health monitoring system for thermoplastic composite structures. The Lamb wave test results are backed up by phased-array inspections, which also provide some extra insight on the internal structure of ultrasonic welds.

1. Introduction

Ultrasonic welding is a very promising technique for joining thermoplastic composite (TpC) components in aircraft primary structures [1–3]. From a mechanical point of view, it allows joints to have high static properties, low through-thickness porosity and lower weight when compared to their fastened counterparts. From a production point of view, the technique has a high potential for industrialisation not only due to short welding times of small joining areas, but also due to the possibility of reliably controlling the process. Villegas [2,3] and Villegas et al. [1] have demonstrated that it is possible to adopt a simple ultrasonic welding setup with flat energy directors (EDs) and use the displacement and power curves from

* Corresponding author at: Structural Integrity and Composites Group, Faculty of Aerospace Engineering, TU Delft, Kluyverweg 1, 2629 HS Delft, The Netherlands.
E-mail address: P.A.ViegasOchoadeCarvalho@tudelft.nl (P. Ochôa).

http://dx.doi.org/10.1016/j.ymssp.2017.06.009
0888-3270/

the sonotrode to monitor the entire process and define the quality of the weld. By stopping the welding process at the maximum power plateau/point, it is possible to maximise lap shear strength for a certain "*material and welding set-up*" combination [2], with the travel at that point consistently corresponding to between 40% and 60% of the thickness of the flat ED. Consistent weld quality can hence be obtained when the welding process is controlled by the displacement of the sonotrode, referred to as welding travel. The cross-section of the optimised ultrasonically welded (USW) TpC joints is characterised by a very thin ($\sim 10^{-2}$ mm) polymeric weld-line between the adherends (consisting of the ED which was not squeezed out of the overlap), and a region within the two laminate layers, adjacent to the weld-line, which is affected by partial fusion of the matrix during the welding process and which extension is determined by the applied force and vibration amplitude [2,3]. Although this heat-affected zone does not have a separation surface as the weld-line, it is expected to have different elastic properties from the rest of laminate. Villegas [2] showed that different welding travel values directly result in different weld-line thicknesses. However, when welds produced with different travels are tested for lap shear strength, different features are observed on the fracture surface. This seems to indicate that travel also affects the effectiveness of intermolecular diffusion between the resin-rich weld-line and the adherends, which is attributed to different times available for heat to be transferred from the ED to the composite substrates.

The introduction of new composite structures in civil aviation has been driving the change towards condition-based maintenance (CBM) as an alternative to the regular inspection interval approach [4]. In turn, CBM has been pushing forward the development of structural health monitoring (SHM) technology capable of reliably assessing the structural integrity of a component during flight or at pre-flight checks. Among all of them, Lamb wave techniques are widely recognised as some of the most promising approaches for SHM of composite structures [5]. In previous work, the authors have investigated barely visible impact damage at multiple locations using Lamb wave techniques [6].

Accurate quantitative diagnostics can only be performed if ultrasonic response changes can be unambiguously correlated to specific damages. That correlation requires the distinction of benign features from damaging ones. Therefore, before designing any SHM system for a component it is first necessary to understand the influence of several intrinsic characteristics of the undamaged joints on Lamb wave propagation.

Most of the research about this problem has been focused on the interaction of Lamb waves with adhesively bonded metallic joints. Rokhlin [7] used theoretical and experimental analysis to show two important facts. First, that multilayer Lamb-type modes can carry ultrasonic energy across an overlap if their mode shapes match well enough with those of the modes in the adherends (which in mathematical terms is measured by the degree of orthogonality between the mode shapes in the two domains [8]). Second, that the sensitivity of Lamb modes to the bond properties depends on the sensitivity of their carrier modes to the same properties. In turn, that sensitivity is determined by the modes shapes in the overlap, which also vary with joint shape. Rokhlin pointed out that if bond inspection is to be performed, then the excitation Lamb mode should be selected such that it is allowed to convert (to some extent) to the necessary carrier modes.

Lowe et al. [9] went deeper into the physics of transmission across lap joints by investigating the mechanism that governs mode conversion at the edges of the overlap. By using finite element analysis and the two-dimensional fast Fourier transform (FFT), they proved that if there are multiple carrier modes, the strength of transmission of the zero-order single-plate symmetric (s0) Lamb mode is determined by their interference when mode conversion occurs at the trailing edge of the overlap. That interference can be mainly constructive or destructive, depending on the relative phases of the carrier modes. The longer the bond and the higher the wavenumber of the carrier modes (which is a function of bond thickness), the larger the phase change during propagation through the overlap, the more constructive the interference, and therefore the stronger the transmission. Therefore, by measuring the transmission coefficient of a certain Lamb mode, it may be possible to detect anomalies in the modal properties of the carrier modes caused by defects in the joint. Later, Lanza di Scalea et al. [10] adopted a fully experimental approach based on air-coupled piezoelectric transducers to study the strength of transmission of the a0 Lamb mode across adhesively bonded aluminium-epoxy-aluminium joints. Not only they were able to confirm the aforementioned carrier mode principles by measuring intermediate (adherend-overlap) transmission coefficients, they were also able to distinguish different bond conditions by measuring overall (adherend-overlap-adherend) transmission coefficients. Additionally, interesting conclusions were drawn about the most adequate frequencies for bond monitoring, with different frequencies being sensitive to different bond states.

With the research by Matt et al. [11] the problem of Lamb wave based SHM of fully composite joints was finally addressed by studying the transmission of the s0 mode across adhesive bonds. The test case was a carbon-epoxy wing skin-to-spar configuration containing areas of different bond condition, namely properly-cured, poorly-cured and disbonded. The specimens were instrumented with permanently attached inter-digital transducers which were used to acquire overall energy transmission coefficients. Changes in ultrasonic strength of transmission allowed three different bond states to be discriminated, although the most sensitive frequency range (100–300 kHz) was considerably lower than the one found in [10] (580–670 kHz) for adhesively bonded metallic joints.

However, TpC joints produced by ultrasonic welding have a unique structure, which properties are considerably different from adhesive bonds and are still not fully understood [12]. Not only the bonding nature is different (intermolecular diffusion [13] instead of adhesion), with unclear influence on the continuity of strain and stress across the overlap, but also the range of bond thicknesses is ten times smaller than in the case of adhesively bonded joints. Consequently, the interactions experienced by guided waves in USW joints fall outside the domain of understanding obtained from previous research.

Therefore the purpose of this paper is to investigate the influence of the welding travel on the transmission of Lamb waves across USW TpC lap shear joints, thereby serving as the first step towards understanding the propagation of guided

waves in this new type of structural systems. A fully experimental approach based on surface-mounted piezoelectric transducers is adopted to test specimens produced with three different welding conditions at two frequencies. After supporting the Lamb wave test results with ultrasonic phased-array inspections of the samples, the observed trends in the time-domain indicators are used to propose a tentative criterion for reliable damage detection in USW TpC joints.

2. Methodology

2.1. Problem statement

If ultrasonic welding is to be used for joining thermoplastic components in aircraft primary structures, intrinsic variability resulting from the manufacturing/assembly process could potentially come from different final overlap thickness. Therefore, a key way to start to understand the propagation of Lamb waves in USW TpC joints is to study the transmission of these waves across overlaps produced with different welding displacement (also called travel).

The approach selected for this research is illustrated by the diagram of Fig. 1, in which the single-lap joint configuration and its main dimensions are shown together with the actuation and sensing positions. By simply varying the welding travel, and assuming there is no difference in heating and cooling rates, the clearest resulting change is the amount of energy director (ED) that is squeezed out of the overlap, and hence the weld-line thickness (WLt). Additionally, some differences in intermolecular diffusion at the welding interface can also be expected, as introduced in Section 1.

Three groups of five USW TpC joints were produced with distinct welding travel values (which selection is described in Section 2.2), instrumented and Lamb wave tested. The results were comparatively evaluated.

2.2. Materials and manufacturing

The plates used in this study were manufactured from Cetex® five harness satin weave carbon fabric reinforced polyphenylene sulfide (CF/PPS) composite semi-preg material, supplied by Ten Cate Advanced Composites. Six layers were stacked according to $[0°/90°]_{3s}$, where [0°] and [90°] correspond to the warp and weft directions, respectively, and subjected to 320 °C and 10 bar for 15 min, resulting in laminates with a nominal thickness of 1.62 mm.

The adherends were water-jet cut out of the plates, with nominal (planar) dimensions of 101.6 mm × 25.4 mm, in order to tightly fit in the ultrasonic welding clamping tool. The longest planar dimension (length) was parallel to the warp direction. This fixture has been designed to allow the production of single-lap joints with an overlap length of 12.7 mm (according to ASTM D1002 [14]), while preventing the movement of the samples during the ultrasonic welding process, which is crucial for the production of joints under fully controlled conditions.

The selection of the welding process parameters was based on the research conducted by Villegas [2,3] and Villegas et al. [1], which has been introduced in Section 1. It was decided to adopt the welding condition that would lead to the maximum lap shear strength as the reference case (which would later be used to acquire the baseline response). Two other conditions were chosen such that they would cover the welding stage during which the ED is molten and starts to flow. The first one is around the beginning of the displacement and power increase, and the second one is between the first and the reference points.

Based on experience acquired by Villegas [2,3], the nominal thickness of the flat PPS ED was chosen to be 0.25 mm, and a force and vibration amplitude of 500 N and 86.2 μm were used, respectively. Within these specifications, a first weld was produced with a travel equal to the ED thickness, in order to obtain the full displacement-power curves (extracted from the ultrasonic welding machine) which are depicted in Fig. 2. With the region of maximum power ending at around 440 ms (point R, of maximum lap shear strength), and the beginning of the displacement increase before 300 ms, the three welding travels to be investigated were defined at 0.12, 0.08 and 0.02 mm (points 1, 2 and 3, respectively, in Fig. 2). Keeping the force and vibration amplitude regimes, and using the 0.25 mm thick ED, three batches of five welded joints were manufactured with the three different travel values.

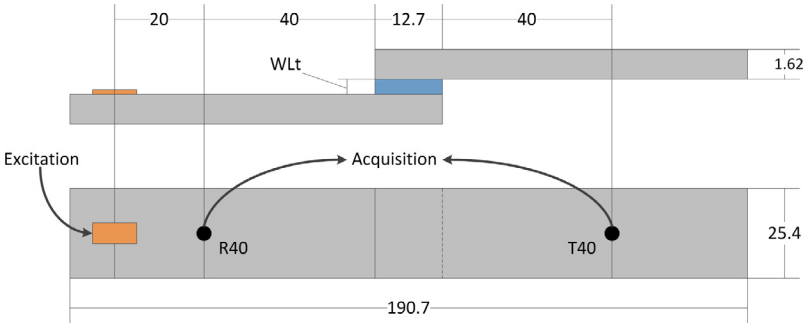

Fig. 1. Diagram of the single-lap configuration to be tested, with main nominal dimensions (in millimetres) and transducer positions. Weld-line thickness is denoted by WLt.

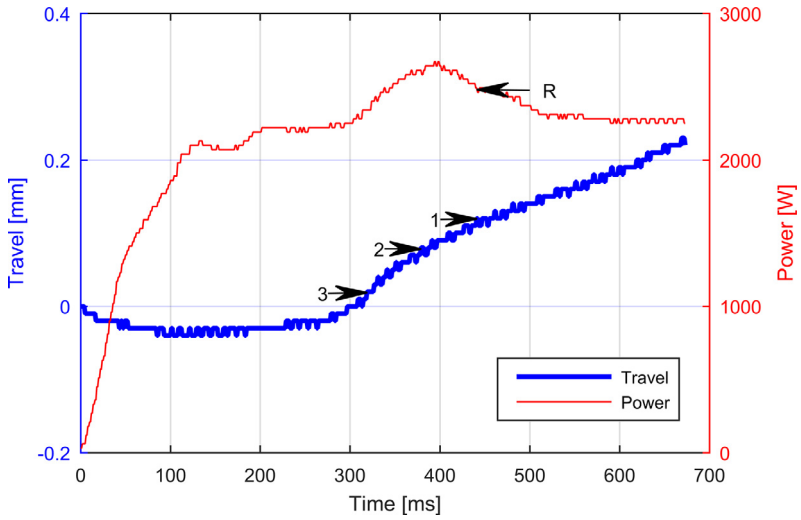

Fig. 2. Ultrasonic welding curves used for process parameter selection.

It is important to note that in the ultrasonic welding procedure used for this research the adherends have to be tightly clamped inside a metal fixture, which is not compatible with having the piezoelectric transducers installed on the adherend surface. This imposes strong limitations in the definition of the baseline, because the same specimen cannot be welded with one travel value, Lamb wave tested, and then welded with another larger travel value. Therefore, it was not possible to have a "pure" baseline. However, since it has been proven possible to use ultrasonic welding to produce thermoplastic composite joints in a controlled and repeatable way [1–3], it was considered appropriate to have three batches of five joints, with those belonging to the group of 0.12 mm welding travel functioning as the reference state.

2.3. Model of dispersive properties

The selection of the excitation regime for the Lamb wave interrogation requires first an analysis of the dispersive properties of the different material systems under research. To this end, the phase and group velocity curves were traced using the DISPERSE™ software, in which the propagation domain had to be simulated. The woven CF/PPS adherends were modelled as an infinite 1.62 mm thick fully anisotropic plate in vacuum, with the nine engineering constants (elastic moduli and Poisson's ratios) defined as by Daggumati et al. [15]. The joints were modelled as infinite layered constructions composed by two 1.62 mm thick CF/PPS plates (with the same properties as before), and one fully connected layer in between representing the weld-line. It is important to note that the programme did not allow intermolecular diffusion between the weld-line and the adherends to be taken into account. As mentioned before, all the weld-line properties were considered to be unaffected by the travel variation except for its thickness. So, the weld-line for each welding condition was modelled as a layer of isotropic material with the elastic properties of the PPS neat resin [16] and the thickness, th_{WL}, calculated according to Eq. (1) by using the mean measured dimensions of the adherends, $\overline{th}_{AD,Left}$ and $\overline{th}_{AD,Right}$, and overlaps, $\overline{th}_{OVER}$ (listed in Tables 1 and 2). The obtained dispersion curves of the adherends are as shown in Fig. 3. The phase velocity curves of the different joint overlaps are compared in Fig. 4.

$$th_{WL} = \overline{th}_{OVER} - \overline{th}_{AD,Left} - \overline{th}_{AD,Right} \tag{1}$$

2.4. Considerations about the excitation

In the scope of this study, it is important to try to establish correlations between the excited mode, its interaction with the structural discontinuities and how it is transmitted across the joint. Thus, the choice of excitation frequency should follow certain criteria in order to enhance signal interpretation [9]. Firstly, the signal should be as simple as possible. Which means

Table 1
Measured dimensions of adherends and energy directors.

	Adherend thickness [mm]		ED thickness [mm]
	Left	Right	
Avg.	1.62	1.63	0.23
StD.	0.02	0.01	0.01

the frequency range should only allow the minimum number of guided modes to be excited, and if possible, a single mode. Secondly, the signal shape should be as independent from the propagation distance as possible, in order to isolate the variables related to the transformation taking place at the joint. Therefore, the modes should be as non-dispersive as possible. Additionally, the excited wavelengths should be small enough to prevent the waves from being in the standing regime. Taking this into account, the first candidate frequencies can be selected. From Fig. 3a) and Fig. 3b) it is possible to observe that below 450 kHz (1st cut-off) only the zero-order modes can be excited in the simple adherends and that their dispersion is

Table 2
Measured overlap dimensions and weld-line thicknesses used in the model.

Travel [mm]	Overlap thickness [mm]		Calculated weld-line thickness [mm]
	Avg.	StD.	
0.12	3.28	0.01	0.03
0.08	3.32	0.01	0.07
0.02	3.37	0.01	0.12

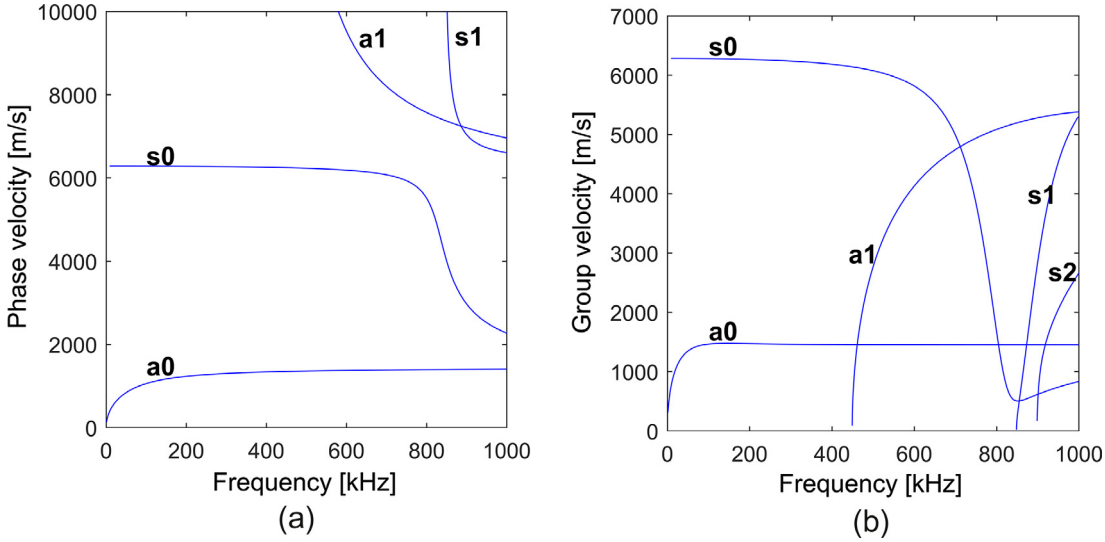

Fig. 3. Dispersion curves for the single CF/PPS plate: (a) phase velocity; (b) group velocity.

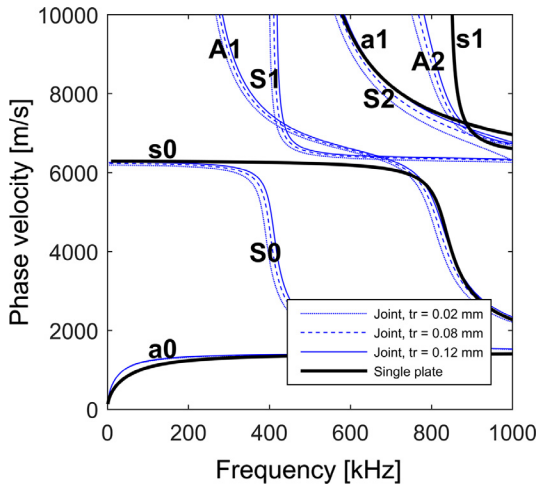

Fig. 4. Phase velocity dispersion curves compared for the different systems (single-plate modes indicated in small letters, multilayer modes indicated in capital letters).

Table 3
Transducer length-to-half-wavelength and transducer width-to-half-wavelength ratios for candidate frequencies.

Frequency [kHz]	200	250	300	350	400
$L/(\lambda_{A0}/2)$ [–]	5.2	6.3	7.4	8.5	9.6
$L/(\lambda_{S0}/2)$ [–]	**1.0**	1.3	1.5	1.8	2.0
$w/(\lambda_{A0}/2)$ [–]	2.6	3.1	3.7	4.2	4.8
$w/(\lambda_{S0}/2)$ [–]	0.5	0.6	0.8	0.9	**1.0**

low (as seen from their low slope at that frequency). One could then select a range of candidate excitation frequencies, between 200 and 450 kHz.

One of the concerns in this research is to use transduction technology which could potentially be applied in real SHM systems. Under this constraint and in an effort to predominantly excite a single mode, it was initially decided to make use of the wavelength tuning effect [17] of piezo-ceramic transducer patches. This property allows a mode to be predominantly excited if the main vibrating dimension of the transducer is equal to an odd multiple of the half-wavelength. The available piezo-ceramic transducers (made from APC material 850, APC International Ltd.) were 0.4 mm thick, 8 mm wide and 16 mm long. The ratio between each of the two in-plane dimensions and the half-wavelength of each zero-order mode was evaluated for several frequencies in the previously selected range, in order to find the odd multiples. As shown by the numbers in bold in Table 3, the condition for wavelength tuning is met only at 200 kHz for the transducer length direction, and at 400 kHz for the transducer width direction. Because the longer the main vibration dimension, the stronger the piezoelectric response of the transducer, it was decided to use the length as the dimension parallel to the wave propagation direction, thereby opting for predominant excitation of the s0 mode at 200 kHz. Moreover, opting for the width as the main vibrating dimension (hence using 400 kHz as centre frequency) would imply exciting the a1 mode.

The main excitation frequency was below the 1st cut-off in both the adherend and the joint cross-section. However, higher-order carrier modes can play an important role in the transmission of energy across the joint [9,11]. Therefore, it was decided to use a second excitation frequency of 250 kHz to allow the A1 carrier-mode to occur in the overlap. While this value remains below the first cut-off in the adherend and is just slightly deviated from the wavelength tuning condition, it is slightly above the 1st cut-off in the overlap, as shown in Fig. 4. The excitation signals used were sinusoidal tone-bursts with five cycles and Hanning amplitude-modulation. These choices allowed a compromise between narrow frequency band and duration, i.e., a compromise between the amount of parasitic frequencies and the level of overlapping of the zero-order modes.

3. Experiments

Lamb wave tests were conducted on the USW specimens according to the set-up shown in Fig. 5. An Agilent 33500B arbitrary waveform generator was used to create five-cycle sinusoidal tone-bursts modulated by a Hanning amplitude window with a maximum value of 8.19 V_{pp}. These signals were transmitted to the specimens at 200 and 250 kHz by APC 850 piezo-ceramic 16 mm × 8 mm × 0.4 mm patches glued to one of the adherends with cyanoacrylate, 60 mm away from the overlap (as illustrated in Fig. 1). The ultrasonic responses were captured by two Mistras WSα general purpose wideband sensors placed 40 mm before and after the overlap. The main propagation direction was considered to be parallel to the length of the specimens, and therefore along the warp direction of the composite fabric (see Section 2.2). The sensors were coupled to the specimens by Sonotech shear gel and adhesive tape, and directly connected to a PicoScope 6402A digital oscilloscope which was operated by a computer.

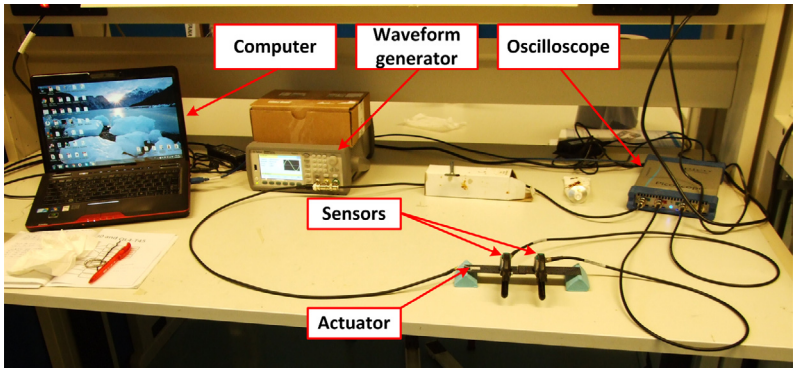

Fig. 5. Experimental set-up used for the Lamb wave tests on the USW specimens.

4. Results and discussion

4.1. Response observation

By observing responses acquired 40 mm after the overlap at 200 and 250 kHz, such as those depicted in Fig. 6A and Fig. 6B respectively, it is not possible to say that the only excited mode was the s0 mode. The existence of multiple overlapping edge reflections, together with joint reverberations, prevents the unambiguous evaluation of any other modes besides the first direct one when using pure time-domain signal processing. Since it is not really possible to actually tune the excitation, both the a0 and s0 modes are considered to be present. Therefore, in order to cope with the impossibility of performing pure mode analysis, the study relies on full response characteristics to understand what the influence of welding travel on the transmission of Lamb waves across USW TpC joints is.

At 200 kHz, the possible carrier modes are A0 and S0, while at 250 kHz the A1 can also exist. In general, it must be assumed that each Lamb mode can convert to any of the carrier modes. However, in reality, a mode is not "*excited if its field distribution is orthogonal to the excitation field.*" [9] Thus, a certain carrier mode will be excited if its mode shape in the lower layer of the overlap is similar to the mode shape in the adherend (before the overlap). Following the same logic, the Lamb modes arriving at the sensor on the other side of the joint are determined by the match between the mode shapes of the excited carrier modes in the upper layer of the overlap and the mode shapes of Lamb mode in the adherend.

Since both the a0 and s0 modes are excited, both A0 and S0 carrier modes will appear in the overlap after mode conversion at the edge of the joint. By mode shape similarity, the a0 mainly converts to A0, and the s0 mainly converts to S0. The A1 carrier mode might play some role in the transmission of the s0 energy across the joint at 250 kHz, since their out-of-plane displacement distributions are both approximately null.

Besides the direct transmission, part of the energy transmitted into the overlap is reflected at the exiting edge with simultaneous mode conversion. The backward-travelling mode undergoes another reflection at the entering edge with new mode conversion, and finally leaves the overlap after mode converting to one of the single-plate modes. This sequence of events is depicted in Fig. 7 and is called a reverberation. The carrier modes can be reverberated more than once, with decreasing amount of energy crossing the overlap each time. So, for the incident s0 mode, the S0 is generated, being then converted to A0 which is again converted to S0, which then converts to s0 when being transmitted outside the overlap. The estimated arrival time of this first reverberation (s0-S0-A0-S0-s0) at both 200 and 250 kHz is around 0.03 ms for all the three welding

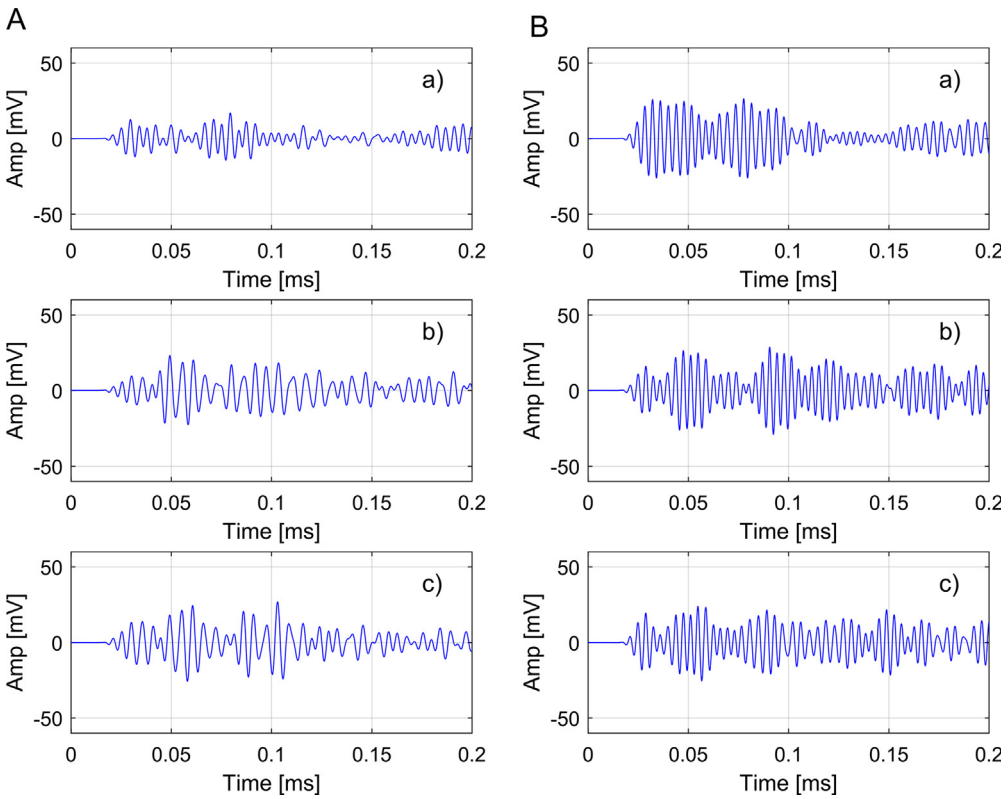

Fig. 6. Responses at T40 position for 200 kHz (A, left side) and 250 kHz (B, right side) excitation, from a specimen produced with welding travel of (a) 0.12 mm, (b) 0.08 mm, and (c) 0.02 mm.

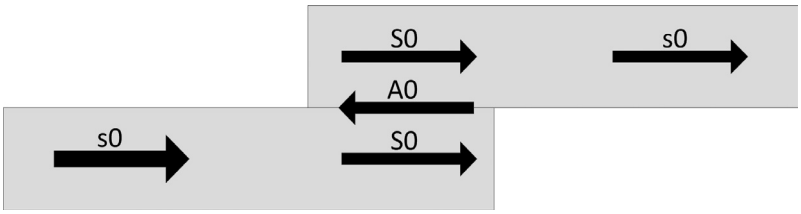

Fig. 7. Diagram of single reverberation after incident s0 mode.

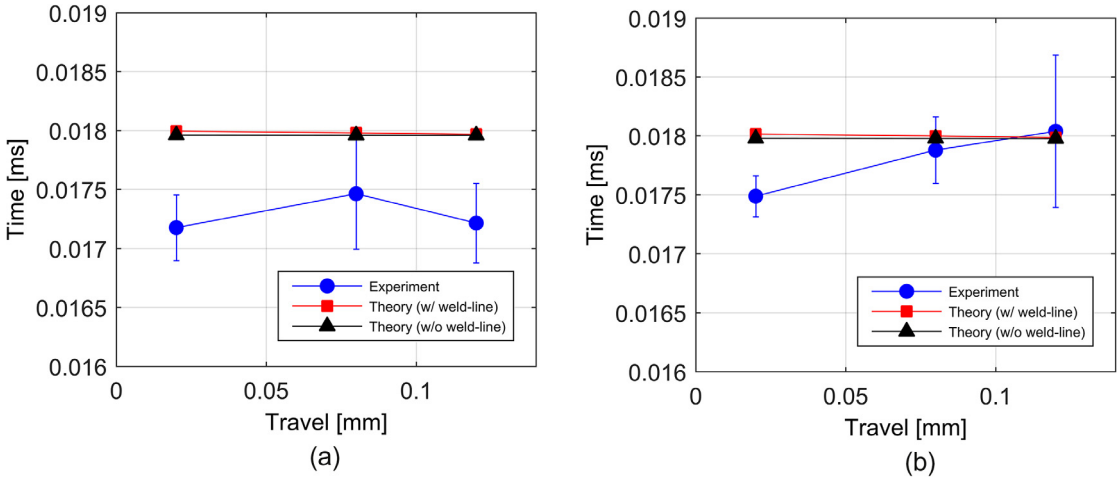

Fig. 8. Onset time of the s0 mode for (a) 200 kHz and (b) 250 kHz.

travels, with minor differences between them. This reverberation group overlaps with the trailing edge of the first arriving s0 group and edge reflections.

4.2. Signal onset

The onset of the signal at the T40 sensor corresponds to the arrival of the directly transmitted s0 mode. According to theory, for the same welding travel (i.e. same joint type), the s0 arrival time follows the evolution of phase velocity with frequency in an inverse way. Thus, for each weld condition, the arrival time is expected to increase when the frequency is raised from 200 to 250 kHz, with the differences lying between 1×10^{-5} and 2×10^{-5} ms (barely noticeable).

For the same frequency, the lower the welding travel, the thicker the overlap (assuming weld-line thickness is the only varying parameter when travel is changed), and hence the lower the phase velocity, which implies a later arrival time. The decrease in phase velocity with increasing weld-line thickness means the average stiffness of the overlap cross-section is in fact decreasing.

The experimental results for the onset time (depicted in Fig. 8) were obtained with the threshold method [18,19], not directly applied to the signal but to the normalised signal envelope. The threshold level was set to 0.46% of the normalised envelope amplitude so that all onsets would be correctly captured. The computed values show some deviations from theory, especially at 200 kHz. Although the average s0 arrival times are higher for 250 kHz than for 200 kHz for all three welding conditions (thereby following the theoretical trend), the experimental values are on average 0.070 and 0.023 μs lower than the theoretical values for 200 and 250 kHz, respectively. Taking the theoretical results as the "true values", then the average relative error was around 3.9% and 1.3% for 200 and 250 kHz, respectively.

One possible explanation for differences between theoretical and experimental results could be that the adopted model overestimates the arrival time of the directly transmitted s0 mode. This would indicate that the actual average stiffness along the entire propagation path is higher than the in the model. The fully anisotropic properties adopted to model the CF/PPS composite material have been proven to accurately describe the laminate used in this research [15], and are in total agreement with the values provided in the CF/PPS material datasheet [16]. However, because there is still no accurate characterisation of ultrasonic weld interfaces, the weld-line was considered as an isotropic layer of neat PPS polymer, with properties taken from the datasheet of the material used in this study [16]. When a rigid connection between two solid layers is chosen, DISPERSE^{TM} assumes the interface is defined by a clear boundary across which there is continuity of displacements and stresses. This means the modelled interface between the composite layer and the weld-line resembles that of a "perfect"

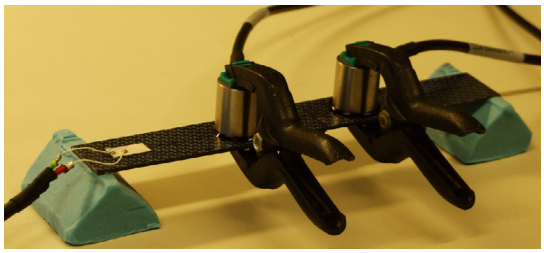

Fig. 9. Detail showing the coupling of the sensors to the surface of the specimens.

adhesively bonded joint, where the two materials are completely "glued" together. However, ultrasonic welding works through fusion bonding which promotes intermolecular diffusion between the materials (actual material mixing), thereby joining them together [3]. Therefore, one could argue that the differences between theoretical and experimental arrival times were due to inaccurate modelling of the properties of the weld interface, which in the present case seems to be stiffer than the modelled one. If the weld-line is then assumed to be normal material of the CF/PPS laminate, and the overlap is modelled as being entirely made of TpC material with a total thickness equal to the value obtained with the corresponding welding condition (as listed in Table 2), then it might be possible to evaluate the effect of considering a stiffer overlap. Comparing the arrival times predicted for these equivalent overlaps with the previously presented theoretical values (also plotted in Fig. 8 as the case "without weld-line"), there is only a small difference between them which is not enough to justify the experimental results.

Another explanation might be in the clamps used to prevent the sliding movement of the sensors on the surface of the specimens, as shown in Fig. 9. By applying pressure on both surfaces, the stiffness of the regions around the sensors might have been slightly increased, thereby allowing for a local increase of wave velocity and consequently a decrease in onset time. To test this hypothesis, Abaqus/Explicit was used to build a finite-element model of the single-lap joint specimens. All the regions were defined as deformable three-dimensional volumes. The nominal dimensions of the adherends were adopted (101.6 mm $\times$ 25.4 mm $\times$ 1.62 mm), together with the nominal overlap distance of 12.7 mm. The composite material of the adherends was modelled as anisotropic homogenous, with the nine engineering constants (elastic moduli and Poisson's ratios) defined as by Daggumati et al. [15]. The weld-line was considered as isotropic homogenous, and its elastic properties equal to those of the PPS neat resin [16]. The weld-line thickness for each welding travel case was defined as described in Section 2.3. The rectangular piezo-ceramic (PZT) actuator patch was modelled as orthotropic homogeneous material, with elastic properties equal to those of APC 850 [20,21], and nominal dimensions of 16 mm $\times$ 8 mm $\times$ 0.4 mm. The mesh was formed by C3D8R elements. In order to respect the Courant-Friedichs-Lewy condition [22], it was always ensured that there were twenty elements per shortest wavelength of the excitation bandwidth in the *xy*-plane (for all the regions). Six elements were defined along the thickness of the adherends, and one element along the thickness of the weld-line and PZT patch. The connection between regions was ensured by tie constraints. The excitation load was introduced by applying distributed forces on the faces of the PZT patch, according to the PZT force model [23]. The value of those forces was computed based on the constitutive equations of piezoelectricity, by using voltage amplitudes in agreement with the experiments, and a sinusoidal tone-burst window with a Hanning amplitude modulation. Finally, the sensor clamp effect was simulated by applying clamping boundary conditions to surfaces on the top and bottom faces of the adherends, at a distance of 40 mm before and after the overlap. Those surfaces had an area equivalent to that of the Mistras WSα general purpose wideband sensors (approximately 283.4 mm^2).

Simulations were performed for the three cases of welding travel and the two excitation frequencies. For each of these travel-frequency pairs, the clamped and unclamped (or free) scenarios were taken into account. Since the acoustic emission sensors used in the experiments are sensitive to velocity (due to construction [24] but also due to coupling with shear gel [25]), the ultrasonic responses after the overlap (location T40 in Fig. 1) were collected as the total velocity at the corresponding sensing node. The signal onset times were extracted with the same threshold method as previously described, and are plotted in Fig. 10a and b, for 200 and 250 kHz, respectively. The graphs show that the numerical signal onset times in the clamped scenario are lower than those in the free scenario, for both frequencies. Moreover, the values are in the same range as those in Fig. 8. Therefore, the numerical results seem to confirm the hypothesis that the sensor clamps are responsible for the experimental signal onset times being lower than the theoretical ones.

In any case, even though it is not possible to draw any conclusions about the material properties of the ultrasonic welds, it seems valid to state that the arrival time of the direct transmission s0-S0-s0 can potentially be used to detect changes in the stiffness of the weld when compared to the pristine state.

4.3. Transmission coefficient

The methods of analysis used in this research do not allow the evaluation of the transmission of each mode individually across the lap joint. However, it is possible to evaluate the efficiency of transmission of the total incident energy, i.e. the

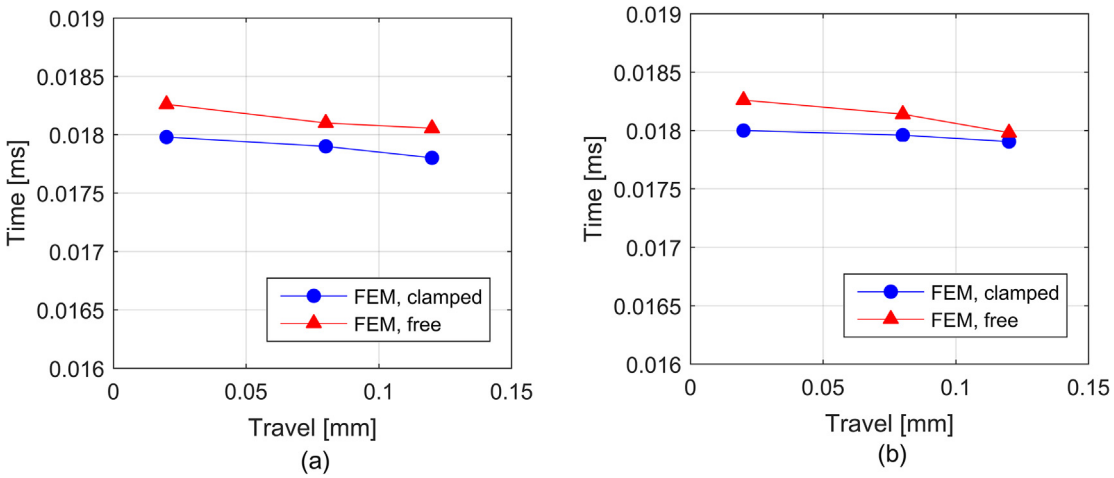

Fig. 10. Numerical results for signal onset with and without clamped sensor boundary conditions for (a) 200 kHz, and for (b) 250 kHz.

transmission of the a0 and s0 Lamb modes together. The power transmission coefficient (PTC) was computed for each specimen of each condition, at each frequency, according to Eq. (2). The incident power for each condition, P_{INC}, at each frequency, was taken as the average of the powers, P_i, of the signals acquired at the position R40 from all specimens, *Nsp*, in each batch, as defined in Eq. (3). Power values for each specimen (including the transmitted power P_{TRANS}) are calculated from the square of the root mean square (rms) level of the signal x whose number of sample points is denoted by *Npts*, as defined in Eq. (4). The experimental results obtained at 200 and 250 kHz are plotted in Fig. 11.

$$PTC = 10\log_{10}(P_{TRANS}/P_{INC}) \tag{2}$$

$$P_{INC} = \sum_{i=1}^{i=Nsp} P_i \Big/ Nsp \tag{3}$$

$$P = 1/Npts \sum_{j=1}^{j=Npts} x_j^2 = rms^2 \tag{4}$$

For both frequencies, the values obtained were between −10 and −15 dB, which corresponds to 10% and 3% of the incident signal power, respectively. These low values are within the expected range, based on the considerations by Lowe et al. [9] about the influence of bond length and bond thickness on the Lamb wave transmission across adhesively bonded lap joints. Since there is only tenuous variations of weld-line thickness and intermolecular diffusion at the weld interface from 0.12 mm to 0.02 mm welding travel, the variation of PTC with that parameter is also small, and with no apparent common

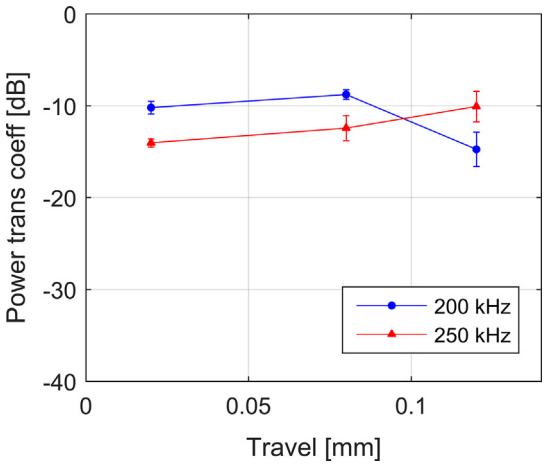

Fig. 11. Variation of PTC with welding travel for 200 and 250 kHz.

trend. At 200 kHz, PTC remains almost constant (around -10 dB) from 0.02 to 0.08 mm travel, and decreases to approximately -15 dB for 0.12 mm travel. At 250 kHz, the coefficient is around −14 dB for 0.02 mm travel, and goes up 2 dB per each change of travel, ending at around −10 dB for 0.12 mm travel. However, bearing in mind that this analysis includes both Lamb modes (a0 and s0) and neglecting (for now) the reverberations of the carrier modes, it may be possible to establish a reason for the observed evolutions. For that it is necessary to consider the displacement mode shapes of the Lamb modes in the adherend (the two leftmost columns) and carrier modes in the overlap (the two and three rightmost columns, for 200 and 250 kHz, respectively) for the three welding conditions, at both excitation frequencies, depicted in Figs. 12 and 13.

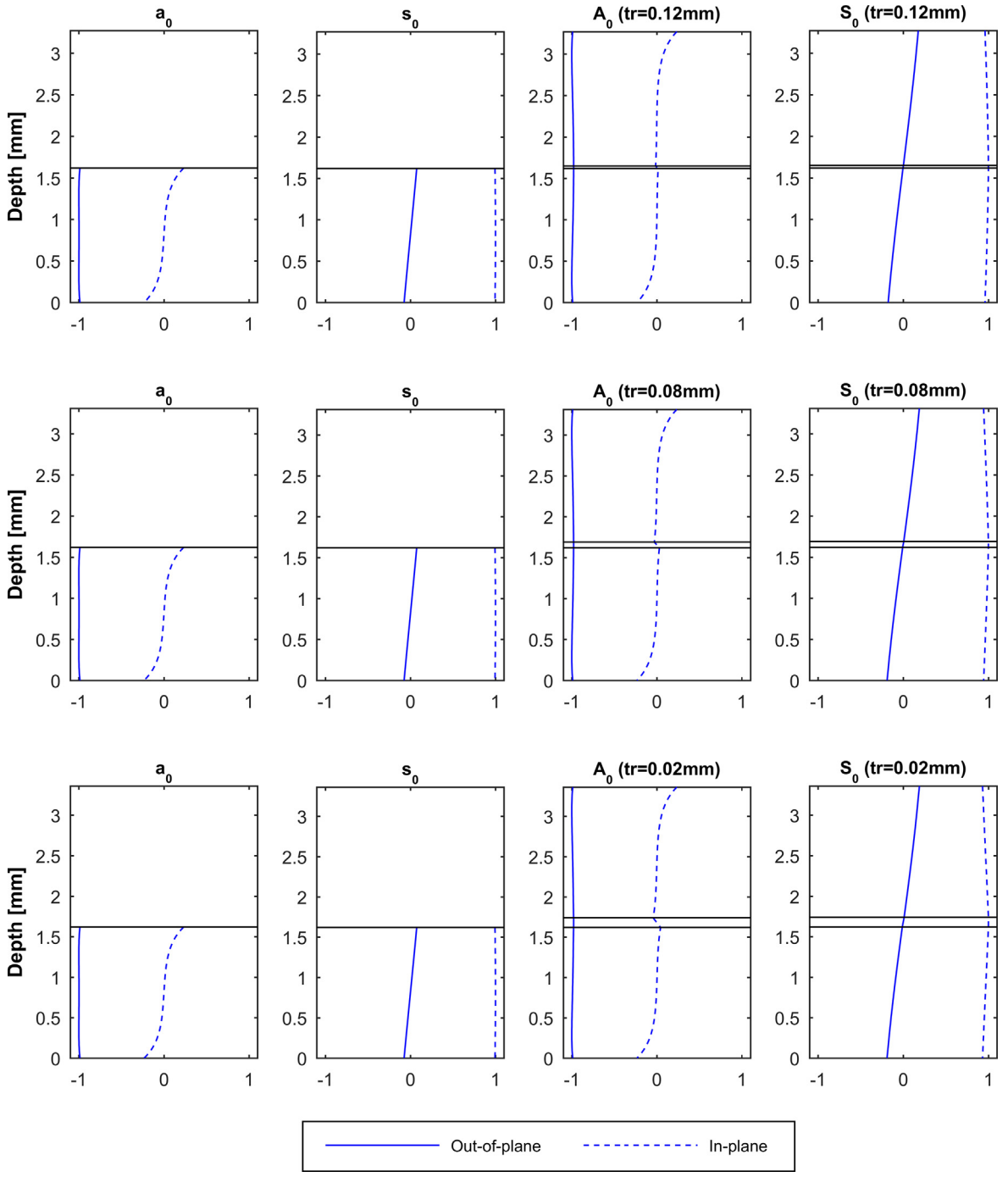

Fig. 12. Displacement mode shapes of a0 and s0 Lamb modes in the adherend and A0 and S0 modes in the overlap, for the three welding travel values, at 200 kHz.

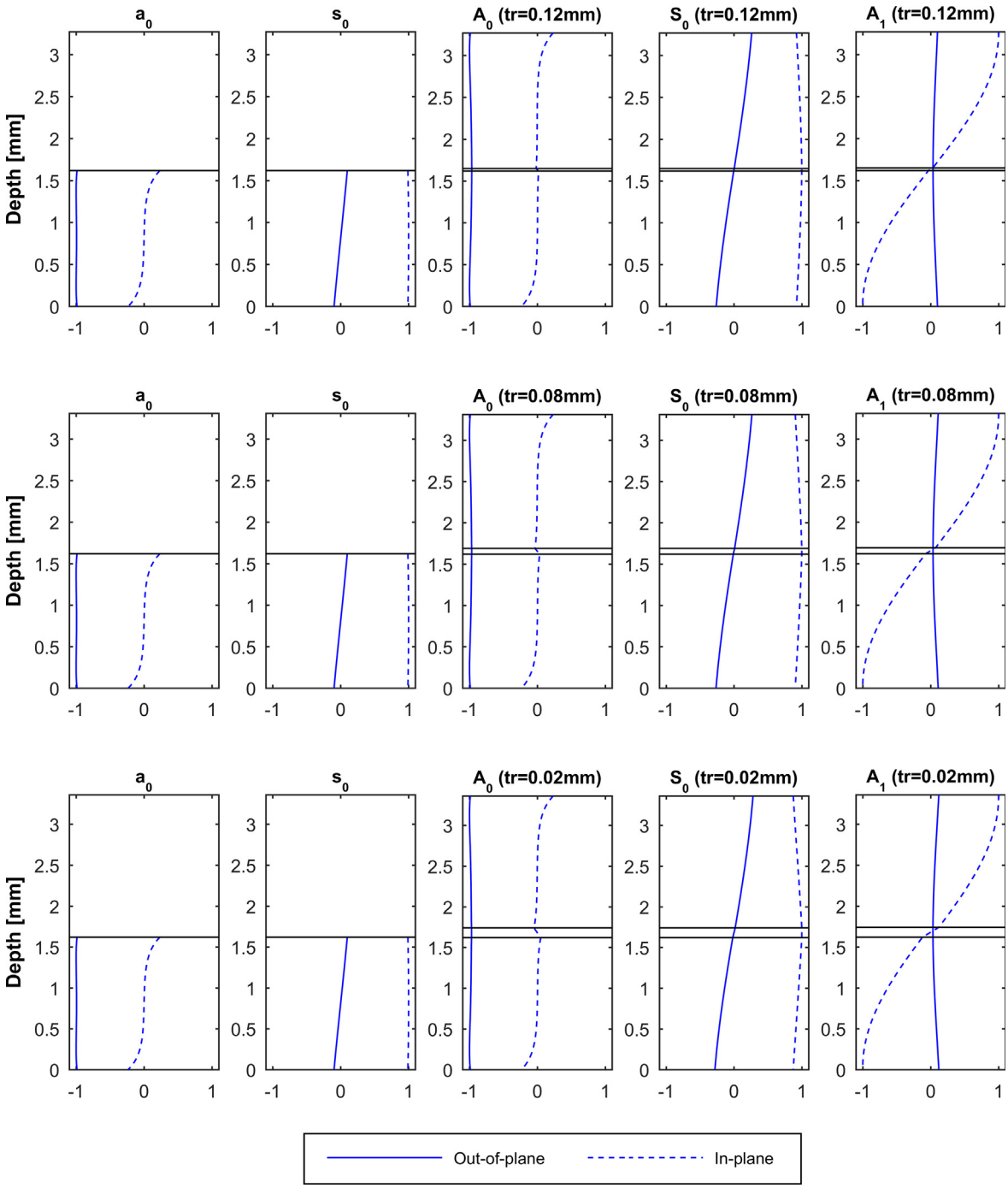

Fig. 13. Displacement mode shapes of a0 and s0 Lamb modes in the adherend and A0, S0 and A1 mode in the overlap, for the three welding travel values, at 250 kHz.

At 200 kHz (see Fig. 12), the a0 and s0 Lamb modes in the adherend can only convert to the A0 and S0 carrier modes in the overlap region. The conversion of the s0 to the S0 mode is expected to have approximately the same efficiency for the three travel values, as the match of the displacement mode shapes is almost unchanged. So, the energy of the transmitted s0 is expected to remain approximately constant for the tested travel values. The same cannot be said for the a0-A0 conversion. As welding travel increases (i.e. weld-line thickness decreases), the curvature of the in-plane displacement distribution in the vicinity of the weld-line decreases, worsening the match between the A0 mode-shape in the lower overlap layer and the incident a0 mode shape in the adherend, thereby decreasing the efficiency of the a0 mode transmission and, in turn,

Table 4
Phase analysis of S0 and A1 carrier modes at 250 kHz (the variations of phase change, $\Delta\varphi$, are the differences to the previous welding conditions).

	250 kHz					
Travel [mm]	0.12		0.08		0.02	
Mode	S0	A1	S0	A1	S0	A1
Total $\Delta\varphi$ [rad]	3.22	1.49	3.24	1.62	3.26	1.75
Variation $\Delta\varphi$ [rad]	0.02	0.13	0.03	0.13		
Variation $\Delta\varphi$ [%]	0.64	8.67	0.82	8.34		

the energy of that mode across the joint. This could explain the reduction of the power transmission coefficient for 0.12 mm travel.

At 250 kHz (see Fig. 13), the same evolution for the a0-A0 conversion is still observed. However, more factors come into play in the transmission of the s0 mode. Since the out-of-plane displacement distribution of the A1 mode in the lower overlap layer is relatively close to that of the s0 mode in the adherend, that overlap mode might also play a role in transmitting the energy across the joint. The velocities of the S0 and A1 modes are quite different, but they still interfere at the end of the overlap, when the second mode conversion back to s0 takes place. That interference can be more destructive or constructive, depending of the relative phase of each carrier mode after travelling the distance equal to the overlap length. According to Lowe et al. [9], two tendencies play a role in determining the nature of the interference. On one hand, the larger the propagation distance, the higher the phase change and the more constructive is the interference at the end of the overlap. On the other hand, the higher the wave number of the carrier mode (dependent on the overlap thickness), the higher the phase change, and the more constructive is the interference.

In this case, where the overlap length is not a varying parameter, the small (and not so different) overlap thicknesses of the three welding travel batches do not promote enough phase change to favour constructive interference (when compared to the phase changes obtained by Lowe et al. [9]), as summarised in Table 4, thereby reducing the efficiency of the s0 mode transmission and the energy of that mode across the joint. Furthermore, as welding travel decreases (i.e. weld-line thickness increases), the change in in-plane displacement distribution of the S0 is noticeable (more curvature), thereby worsening the match with the adherend s0 mode shape. These two occurrences together could explain why the power transmission coefficient for 0.02 mm is lower than at 200 kHz.

As travel goes up, the match between the s0 and the S0 mode shapes improves, and the efficiency of conversion from s0 to S0 and back increases, therefore increasing PTC to −10 dB. It is worth noticing that, due to the balance between the two (contrary) evolutions for the a0-A0 and s0-S0 conversions, the rate at which the PTC increases at 250 kHz for the whole range of travel values (27 dB/mm from 0.02 to 0.08 mm, and 59 dB/mm from 0.08 to 0.12 mm) is lower than the rate at which it decreases at 200 kHz from 0.08 to 0.12 mm (149 dB/mm).

Although transmission phenomena are frequency dependent, overall PTC seems to be relatively insensitive to differences in welding travel at the tested frequencies. Hence, it was decided to further elaborate on the evolution of this relationship with frequency. For that it is first important to pay attention to the bandwidth of the excitation signal. The excitation tone-burst does not have only one frequency component, but a finite frequency band. Most of the energy is transmitted at the centre frequency (which can also be called as nominal excitation frequency), although there is always some energy which is transmitted though modes excited at all the other side frequencies. The bandwidth is determined by the type of amplitude modulation and the number of cycles of the tone-burst [26]. If one would want to create an excitation at the maximum possible frequency without generating any higher order mode in the adherends, then the bandwidth upper limit should not go beyond the first cut-off frequency, which is approximately 449 kHz for the TpC laminate used in this research (see Fig. 3). In the case of a 350 kHz five-cycle sinusoidal tone-burst with amplitude modulation by a Hanning window, the bandwidth would be [154; 546] kHz. Clearly, this signal would excite the a1 mode, therefore the number of cycles should be increased to ten so that the bandwidth would become [252; 448] kHz. If the excitation were to be generated at a higher centre frequency, then an even higher number of cycles would have to be used, which would make the signal more complex and difficult to interpret. Therefore, taking into account these constraints, 350 kHz can be considered as the maximum advisable excitation frequency for the type of material system used in this research. The displacement mode shapes at that frequency, plotted in Fig. 14, can then be used to make some estimates.

The a0 and s0 distributions in the adherend (the two leftmost columns) show little variation when compared to 200 and 250 kHz (Fig. 12 and Fig. 13, respectively). Also the A0 distribution in the overlap region remains almost the same, with the out-of-plane displacement mode shape showing slightly more curvature than at 250 kHz. So, the efficiency of a0-A0 conversion, and in turn the a0 transmission across the overlap, would probably show the same trend with welding travel as previously described, although with lower transmitted power than at 250 kHz.

The same double s0 transmission mechanism explained for 250 kHz is also present at 350 kHz, although in this case, the match of the s0 and S0 mode shapes is worse due to a higher curvature of the S0 in-plane displacement distribution and a larger deviation from zero of the S0 out-of-plane displacement distribution. The larger mode shape dissimilarity between s0 and S0 modes together with the destructive interference of the S0 and A1 modes at the end of the overlap (i.e. when mode converting to s0) would probably result in a PTC value for 0.02 mm travel lower than at 250 kHz. Then, since the s0-S0 mode

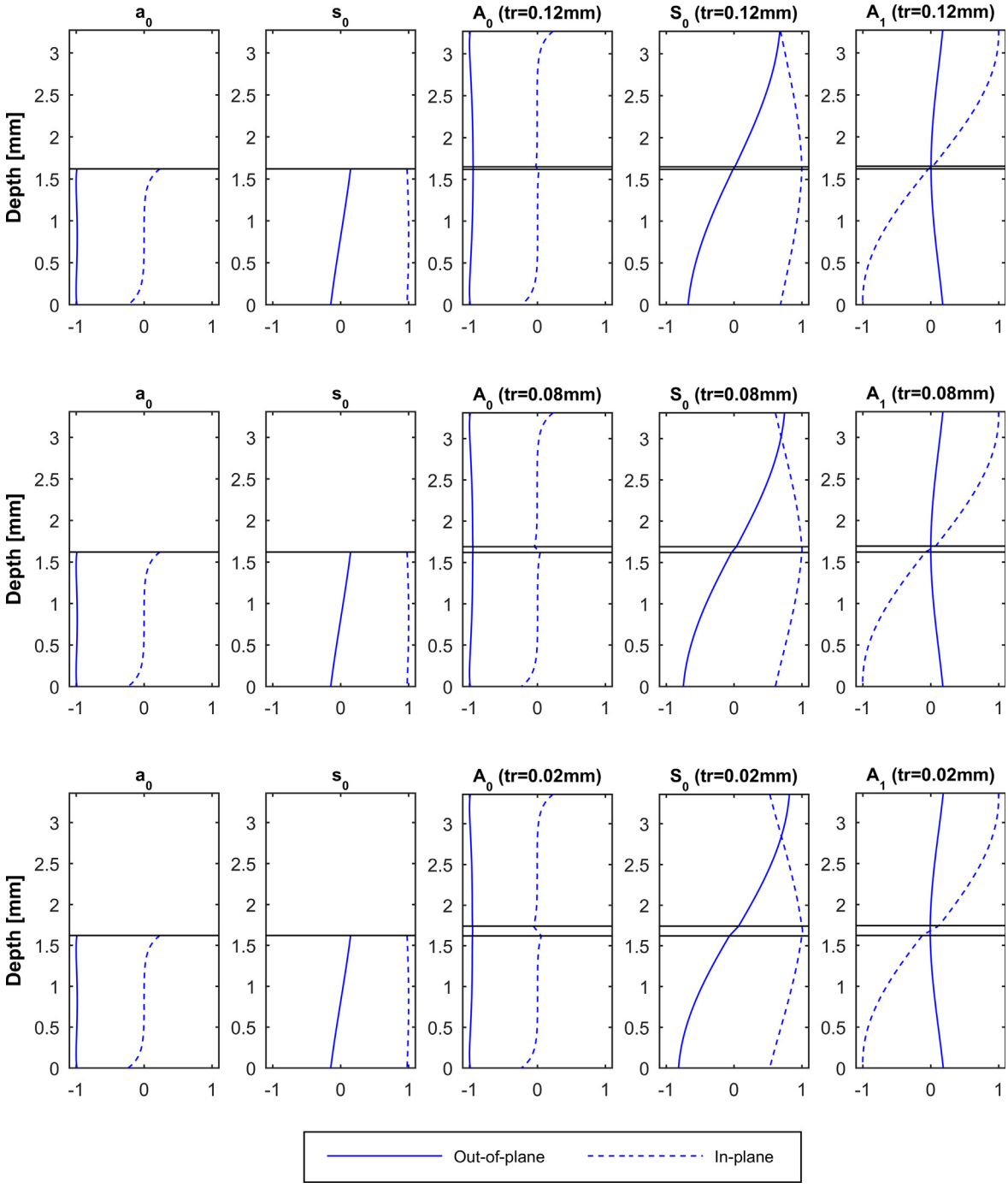

Fig. 14. Displacement mode shapes of a0 and s0 Lamb modes in the single-plate and A0, S0 and A1 modes in the overlap, for the three welding travel values, at 350 kHz.

shape matching slightly improves with increasing welding travel (due to a small reduction of curvature of the distributions), and since there is little variation of phase change with welding travel (as summarised in Table 5), the efficiency of s0-S0 conversion would increase with welding travel at a low rate. Therefore, it seems valid to state that the PTC at 350 kHz would have the same evolution with welding travel, although with some offset to slightly lower values. In the presence of damage in (or around) the joint, the power transmission coefficient would be expected to go down to -30 dB or even lower [10].

Table 5
Phase analysis of S0 and A1 carrier modes at 350 kHz (the variations of phase change, Δφ, are the differences to the previous welding conditions).

	350 kHz					
Travel [mm]	0.12		0.08		0.02	
Mode	S0	A1	S0	A1	S0	A1
Total Δφ [rad]	4.64	3.46	4.71	3.52	4.81	3.58
Variation Δφ [rad]	0.07	0.06	0.11	0.07		
Variation Δφ [%]	1.41	1.72	2.24	1.93		

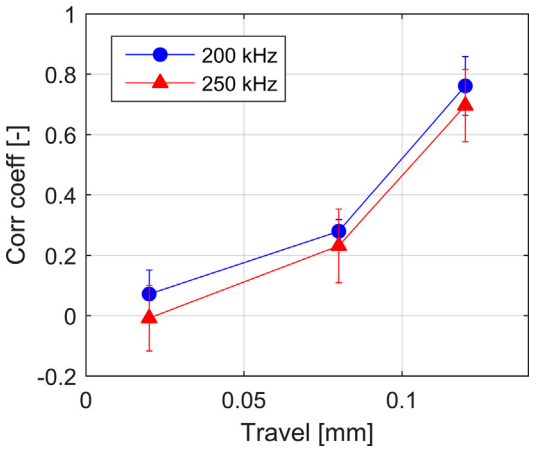

Fig. 15. Variation of CC of the signals with welding travel at 200 and 250 kHz.

4.4. Correlation coefficient

In the attempt of understanding more about the transmission of Lamb waves across USW TpC joints, and thereby further characterising this new type of structures, it was decided to analyse the correlation coefficient (CC), which allows the quantification of the difference between two signals. As presented in Eq. (5), it was decided to correlate the signals from specimens of each condition (S) with a time-domain baseline signal representing the 0.12 mm travel condition (S^0). This time-domain baseline is defined as the average signal computed with the five signals extracted from the specimens of 0.12 mm travel batch. Note that the "bar" above the variable denotes mean value of all signal sample points. The results for 200 and 250 kHz are plotted in Fig. 15.

$$CC = \sum_{i=1}^{i=Npts} (S_i - \overline{S})(S_i^0 - \overline{S^0}) \cdot \left(\sum_{i=1}^{i=Npts} (S_i - \overline{S})^2 \sum_{i=1}^{i=Npts} (S_i^0 - \overline{S^0})^2 \right)^{-\frac{1}{2}} \quad (5)$$

Following from the formula, the larger the deviation from unity, the worse the match of the signal with the baseline. Keeping this in mind, at 200 kHz it is possible to observe a 72% difference for 0.08 mm travel and 93% for 0.02 mm travel, while at 250 kHz differences of 77% and 100% are observed for 0.08 and 0.02 mm travel, respectively. This trend shown for both frequencies indicates that CC is a much more sensitive parameter to welding travel variations (i.e. combined changes of weld-line thickness and intermolecular diffusion at the weld interface) than PTC. The existence of small PTC variations and large CC variations for the same welding travel values indicates that, at the tested frequencies, the differences between batches of signals are not only due to amplitude (i.e. energy content) changes, but also, and mainly, due to shape changes, as it can be understood from simple visual comparison of the responses in Fig. 6A and B.

From specimen to specimen there is unavoidable experimental variability due to small differences in transducer coupling and alignment, sample dimensions and fibre alignment. The coupling influences the captured signal amplitude, while the alignment and geometry influence the incident and reflected fields, and thereby the scatter pattern. Thanks to the adopted baseline definition, it is possible to approximately assess the influence of this inherent experimental variability by looking at CC for the 0.12 mm travel, which correspond to 24% and 31% for 200 and 250 kHz, respectively. Besides being partially incorporated into the baseline definition by the averaging process, these factors are always present for all specimens of the three welding conditions, and therefore they are not responsible for the large deviations in CC. In fact, even if the standard deviation of the data points is taken into account, the variation in CC is still considerably more pronounced than in the case of the PTC parameter.

What differs on a material scale from one welding travel batch to the other is the weld-line thickness and the effectiveness of intermolecular diffusion at the weld interface (as mentioned in Section 1). The previously observed trends for the influence of weld-line thickness on the direct transmission of the modes also apply to the transmission of the reverberated

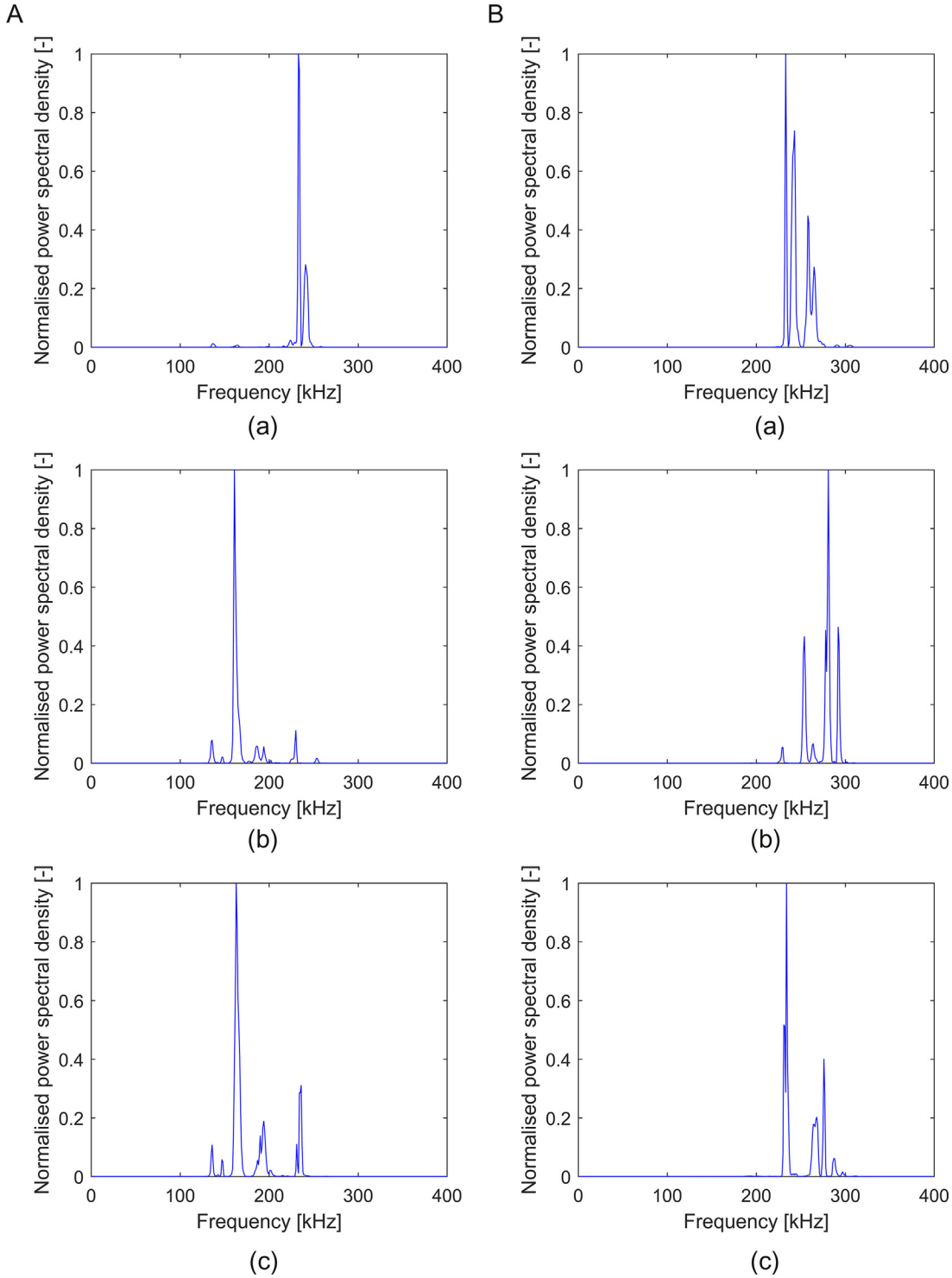

Fig. 16. Normalised power spectral density for 200 kHz (A, left side) and 250 kHz (B, right side) excitation frequencies, from one specimen with welding travel of (a) 0.12 mm, (b) 0.08 mm, and (c) 0.02 mm.

signals. The reverberation wave packets have always lower amplitude than the main signal, so the result of changes in their transmission efficiency becomes much more clear in the interference pattern caused by the their superposition with the directly transmitted wave packets. Thus, at 200 kHz, the transmission efficiency of reverberations of the A0 carrier mode increases when welding travel decreases (i.e. weld-line thickness increases), while the reverberation behaviour of the S0 carrier mode remains approximately the same. This means the interference pattern caused by the superposition of the direct signal and the S0 reverberations does not change, but the one caused by the superposition of the direct signal and the A0 reverberations does. At 250 kHz, not only the A0 reverberation transmission becomes more efficient when travel is reduced, but also S0/A1 reverberation transmission becomes less efficient, thereby inducing a larger deviation from the baseline reverberation pattern than at 200 kHz.

In the normalised power spectral density curves from a specimen of each welding condition for 200 and 250 kHz excitation frequencies in Fig. 16A and B, respectively, it is possible to identify several local maxima caused by interference between the directly transmitted signal, reverberations [9] and edge reflections. As a result, the frequency of maximum power spectral density does not correspond to the excitation frequency. The influence of welding travel on signal interference can be assessed by the changes in the pattern of spectrum local maxima with welding travel. To quantify those differences, the correlation coefficient was computed between power spectral density curves of every specimen of all welding conditions and that of a frequency-domain baseline. That frequency-domain baseline is defined as the average power spectral density computed with the five spectra from the specimens of the 0.12 mm travel batch. The power spectral density CC values compiled in Fig. 17 are in agreement with the trends observed in Fig. 15, and thereby seem to corroborate the hypothesis that, at the tested frequencies, difference in interference between direct signal and reverberations is the main effect of variations of welding travel on Lamb wave response.

4.5. Non-destructive inspections

The results presented so far have been analysed assuming that specimens from the same welding travel batch have the same internal characteristics in the overlap region. However, if this were not true, the above developed reasoning could be invalid. Therefore, in order to ensure there were no significant changes in effectiveness of intermolecular diffusion within each batch of welded joints which could compromise the previous results, it was decided to inspect all the samples with an Olympus OmniScan SX ultrasonic phased-array system at 5 MHz, using a 5L16-A10 probe mounted on a SA10-0L wedge. The coupling between the probe and the wedge was ensured by ultrasonic testing oil, and between the wedge and the sample by Sonotech Sonotrace ultrasonic couplant gel.

The results of the inspections are summarised in Fig. 18, which shows A- and B-scans from specimens which were considered representative of each welding condition. The A-scan (on the left) shows the reflections of the ultrasonic beam from interfaces along the thickness under the centre point of the probe-wedge assembly. The B-scan (on the right) shows the reflections of the ultrasonic beam from interfaces occurring in the cross-sectional area under the probe-wedge assembly defined by the thickness of the inspected medium and the length of the probe. The reflection magnitude is indicated in percentage in the horizontal axis of the A-scan and is matched with the vertical colour scale in the B-scan.

The bi-dimensional view of the overlap cross-section is delimited by the first and third reflections, which indicate the top and bottom surfaces, respectively. The second, weaker, reflection corresponds to the weld interface. The magnitude of the reflection from the top surface is approximately always the same for all specimens, since it is the reflection that takes place when the ultrasonic beam enters the overlap. Contrary, the magnitude of the third reflection (from the bottom surface) varies in an inverse way with the magnitude of the weld interface reflection, i.e. it becomes stronger when the latter becomes

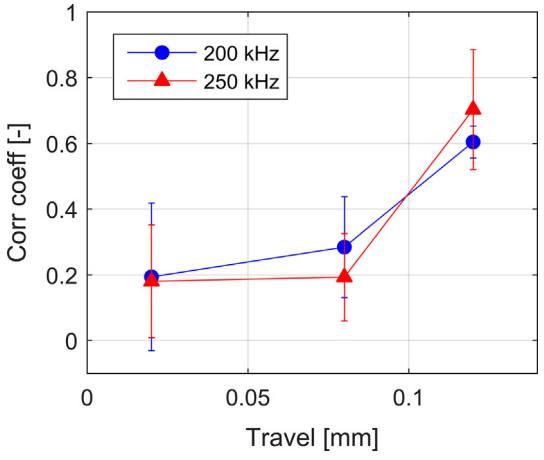

Fig. 17. Variation of the correlation coefficient of the power spectral density curves with welding travel at 200 and 250 kHz.

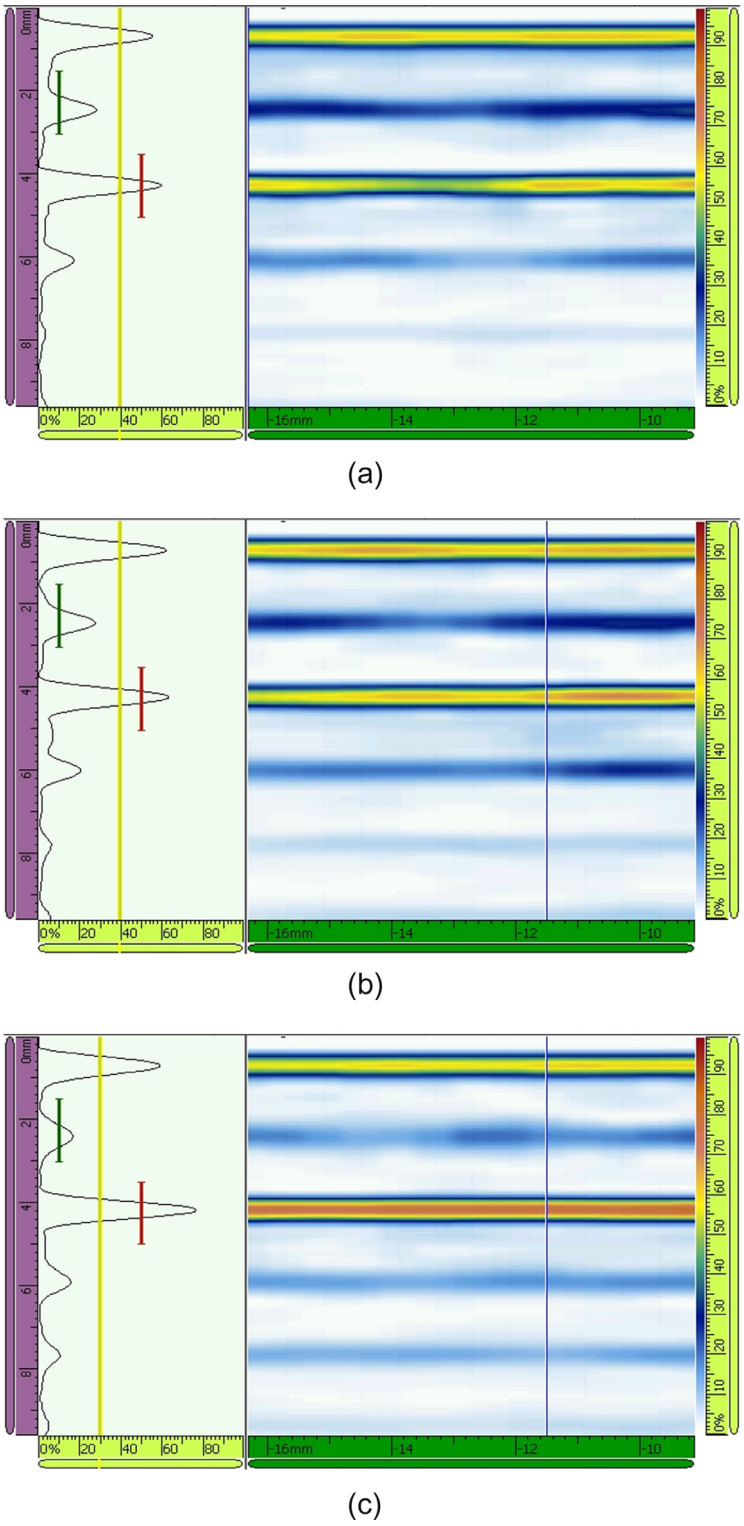

Fig. 18. A- and B-scans from 5 MHz phased-array inspections of a representative specimen produced with a welding travel of (a) 0.02 mm, (b) 0.08 mm, and (c) 0.12 mm. The A-scan percentage scale matches the B-scan colour scale (the closer to red, the stronger the reflection, the closer to white, the weaker the reflection).

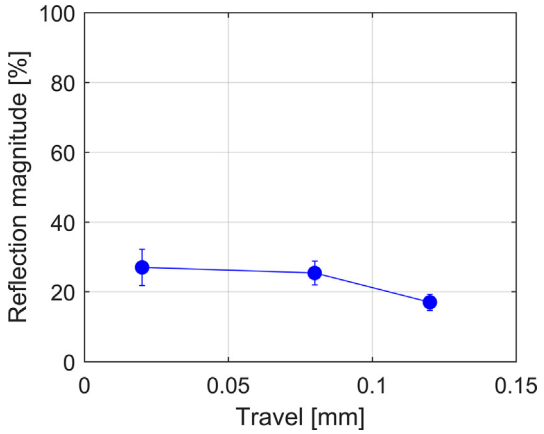

Fig. 19. Variation of the maximum magnitude of the weld interface reflection with welding travel, (extracted from A-scans of the phased-array results at 5 MHz).

weaker. The small peaks after the third reflection correspond to reverberations of the beam inside the cross-section, and can be seen as "copies" of the first three.

In order to quantitatively correlate the results of the phased-array inspections with the welding conditions, the A-scan reflection magnitudes were read for all the specimens and translated into the graph of Fig. 19 which illustrates the strength of the weld interface reflection peak as a function of welding travel. Little differences are found between 0.02 and 0.08 mm travel, with the weld interface reflecting 27% and 25% of the energy transmitted across the top surface, respectively. These are the cases where the weld interface reflection has a "blue" magnitude in the B-scan of Fig. 18a and b. However, from 0.08 to 0.12 mm a significant drop to 17% is observed, revealing the existence of a turning point in the properties of the weld interface. This is visible in Fig. 18c), where the weld interface reflection is mostly "light blue".

It is interesting to note that the width of the weld interface reflection lobe at 10% magnitude barely changes with welding travel (from 0.6 mm for 0.02 and 0.08 mm, to 0.4 for 0.12 mm). That might be due to a combination of the type of filter used by the OmniScan to smoothen the A-scan curves, and the fact that the ultrasonic beam at 5 MHz does not have enough resolution to capture the actual differences in weld-line thickness, since the longitudinal bulk wavelength at 5 MHz is between 0.6 and 1.2 mm, which is considerably above the weld-line thicknesses encountered in the overlaps. Therefore, it is not possible to directly assess the actual differences in weld-line thickness obtained by using different welding travel. In that sense, the direct verification of the squeezed-out status of the energy director cannot be made. However, it is still possible to perform an indirect evaluation.

Contrary to the laminate, where fibres and polymer are mixed, the weld-line is a fibre-free region and, as such, it constitutes an interface from which ultrasounds are always reflected, independently of its thickness. In other words, even when very thin, the weld-line is always a purely polymeric region, and thereby a discontinuity in the overlap. Moreover, welding travel seems to affect the effectiveness of intermolecular diffusion between the weld-line and the adherends, as summarised in Section 1. Taking this reasoning into account, the evaluation of the second reflection peak shows that the larger the welding travel, the less discontinuous is the overlap cross-section. In other words, the larger the welding travel, the more similar to the adherend polymer-rich regions the weld-line becomes. Therefore, it seems valid to say that the lower the second reflection peak, the stronger the intermolecular diffusion between the weld-line and the adherends. The obtained reflection magnitude differences are in agreement with the observations of Villegas [1–3], as they confirm, on one hand, that the effectiveness of intermolecular diffusion at the weld interface increases with welding travel, and on the other hand that it is possible to produce thermoplastic composite welds in a totally repeatable and controlled way by using the developed ultrasonic welding technique. More importantly, these non-destructive inspections show the consistency of the internal properties of specimens within each welding travel batch, thereby supporting the conclusions drawn from the Lamb wave tests. In particular, the low standard deviation observed in Fig. 19 for the welds produced with a welding travel of 0.12 mm provides extra confidence on the baseline definition.

4.6. Contribution to health monitoring applications

In this study it has been shown that the effect of welding travel variations on Lamb wave transmission across ultrasonically welded (USW) thermoplastic composite (TpC) joints is mainly felt on the reverberation pattern and its interference with the directly transmitted wave packets, rather than only on the amplitude of the signal transmitted across the weld. Therefore, both amplitude and phase information should be included if this type of assessment is to be performed for structures with this type of joints. For now the validity of these findings can only be ensured for the type of composite material used in this research, and for excitation frequencies below the first cut-off of the adherends.

Table 6
Values of the proposed DI for the studied welding travel variations.

ΔTravel [mm]	200 kHz		250 kHz	
	DI avg [–]	DI std [–]	DI avg [–]	DI std [–]
0.02–0.08	0.277	0.194	0.285	0.434
0.08–0.12	-2.820	0.748	0.958	0.414

Having confirmed the consistency of the welds produced with each of the three different welding travels, and thereby backed the Lamb wave results, it is now possible to propose an application for the knowledge built in the research. One key issue when performing structural health monitoring (SHM) is the level of confidence with which occurrences are detected [27]. Baseline measurements of the pristine state of the structure (as out of the final production line) include the effect caused by intrinsic variability in the manufacturing or assembling process (e.g. differences in weld-line thickness) on the signal. So, when subtracting the baseline from the altered state, the differences should reveal the presence of damage. The principle behind residual time-trace analysis is to eliminate all the scattering from benign features in the structure, keeping only that caused by new (potentially damaging) occurrences. However, a single damage indicator (DI) might not be enough to distinguish critical from non-critical occurrences, as demonstrated in Sections 4.3 and 4.4. Therefore, an alternative approach to improve the level of confidence is to use a combination of DIs [21,28,29]. As previously analysed, power transmission coefficient (PTC) seems to be considerably less sensitive to different welding travels than correlation coefficient (CC). Thus, based on these parameters Eq. (6) can be adopted in order to establish a tentative criterion in order to unambiguously detect damage in ultrasonically welded thermoplastic composite joints with similar characteristics to those used in this research, using zero-order Lamb wave interrogation. The DI values computed for each welding travel change are presented in Table 6.

$$DI = \Delta PTC \times \Delta CC \tag{6}$$

An hypothetical damage detection case could be as follows. A structure undergoing a final assembly operation in which two components are assembled together by ultrasonic welding at multiple spots. It is possible to imagine that the welds could be produced with slightly different travel values (e.g. due to small misalignments of the setup, due to non-ideal contact between the sonotrode and the overlap, or due to small oil pressure variations in the piston driving the sonotrode), which would result in slightly different material properties for all the joints. In turn those non-damaging changes would not be easily detected in non-destructive inspections. When such component would start to be monitored by a Lamb wave based SHM system (as conceived in this research), and the DI from the several welded spots would be compared among all of them, the values would remain below a certain threshold because the behaviour of the PTC (as described in Section 4.3) would counteract the more "volatile" behaviour of the CC. However, if one of the joints would suddenly have internal damage, the influence of the sensitive CC together with a larger variation of the PTC would ensure the DI value would go beyond the threshold. The DI results can then be classified as shown below:

- Low DI → No damage
- High DI → Damage

The next step in this research is precisely to evaluate the errors of the proposed DI and define appropriate thresholds by testing cases with actual damage in or around the joint.

5. Conclusions

This research focused on studying the influence of one of the main parameters of the ultrasonic welding process, the welding travel, on the transmission of Lamb waves across TpC single-lap joints. Batches of five joints were manufactured with three different overlap thicknesses by varying the welding travel and keeping all the other process parameters constant. Lamb wave tests were performed by exciting only the two zero-order modes on one of the adherends and acquiring the response signal after the overlap.

The signal onset proved to be sensitive to small, local stiffness variations. This means it can potentially be used to detect changes in the stiffness of ultrasonic TpC welds, as long as the coupling conditions between the transducers and the specimens are constant. The absolute value of those changes, and hence the quality of the assessment, depends not only on the onset picking algorithm, but also, and mostly, on the sensors being unobtrusive so that the disturbance of the installation on the acquired signals is minimal.

For the range of thicknesses with which USW TpC joints are typically produced (with the currently available technology), and if Lamb wave interrogation of the type of TpC material system used in this research is performed with a frequency at which only zero-order modes are excited, then the effect of welding travel on Lamb wave transmission is mainly felt on the reverberation pattern and its interference with the directly transmitted wave packets, rather than only on the amplitude of the signal transmitted across the weld. As a consequence, the power transmission coefficient (PTC) is almost insensitive to

different welding travel, while the correlation coefficient (CC) is capable of indicating the signal shape changes due to both amplitude and reverberation differences caused by small variations of weld-line thickness and intermolecular diffusion at the weld interface.

The validity of these conclusions was backed up by ultrasonic phased-array inspections which showed that joints of the same welding travel batch have consistently similar internal structure. An evaluation of the weld interface reflection magnitude confirmed that the larger the welding travel, the more effective the intermolecular diffusion between the weld-line and the adherends. In turn, these inspections also allowed the quantitative benchmarking of the different welding conditions (i.e. travel) against their phased-array response, which can ultimately help improving the characterisation of the ultrasonic welding process.

Based on the trends observed in this study, a tentative criterion was proposed in order to allow quantitative health monitoring of USW TpC joints with a relatively high confidence level. Since damage in (or around) the overlap is expected to affect the PTC much more significantly than welding travel differences, damage could be reliably diagnosed if a large variation of PTC was detected in combination with a large variation of CC.

This study is of crucial importance for SHM of USW TpC joints, since it shows that Lamb waves are sensitive to manufacturing-related variations that can occur in undamaged joints, depending on the calculated indicator. The conclusions of this study can potentially be used for a more adequate selection of the damage index and corresponding threshold in diagnostic, thereby being a valuable contribution for reducing the occurrence of false positives, and ultimately for increasing the reliability of Lamb wave based SHM systems for carbon-fibre reinforced thermoplastic structures assembled by ultrasonic welding.

Acknowledgments

This research is part of the Thermoplastic Affordable Primary Aircraft Structure 2 (TAPAS2) project, financed by the Netherlands Enterprise Agency of the Ministry of Economic Affairs. The authors would like to thank Ten Cate Advanced Composites in the Netherlands for providing the necessary composite material.

References

[1] I. Fernandez Villegas, B. Valle Grande, H.E.N. Bersee, R. Benedictus, A comparative evaluation between flat and traditional energy directors for ultrasonic welding of CF/PPS thermoplastic composites, Compos. Interfaces 22 (8) (2015) 717–729.
[2] I. Fernandez Villegas, In situ monitoring of ultrasonic welding of thermoplastic composites through power and displacement data, J. Thermoplast. Compos. Mater. 28 (1) (2015) 66–85.
[3] I. Fernandez Villegas, Strength development versus process data in ultrasonic welding of thermoplastic composites with flat energy directors and its application to the definition of optimum processing parameters, Compos.: Part A 65 (2014) 27–37.
[4] L. Wenk, C. Bockenheimer, Structural health monitoring: a real-time on-board 'stethoscope' for condition-based maintenance, Airbus Technical Magazine, Flight Airworthiness Support Technol. 54 (2014) 22–29.
[5] Z. Su, L. Ye, Y. Lu, Guided Lamb waves for identification of damage in composites structures: a review, J. Sound Vib. 295 (2006) 753–780.
[6] P. Ochôa, V. Infante, J.M. Silva, R.M. Groves, Detection of multiple low-energy impact damage in composite plates using Lamb wave techniques, Compos. B 80 (2015) 291–298.
[7] S.I. Rokhlin, Lamb wave interaction with lap-shear adhesive joints: theory and experiment, J. Acoust. Soc. Am. 89 (6) (1991) 2758–2765.
[8] J.J. Ditri, Some results on the scattering of guided elastic SH waves from material and geometric waveguide discontinuities, J. Acoust. Soc. Am. 100 (5) (1996) 3078–3087.
[9] M.J.S. Lowe, R.E. Challis, C.W. Chan, The transmission of Lamb waves across adhesively bonded lap joint, J. Acoust. Soc. Am. 107 (3) (2000) 1333–1345.
[10] F. Lanza di Scalea, P. Rizzo, A. Marzani, Propagation of ultrasonic guided waves in lap-shear adhesive joints: case of incident a0 Lamb wave, J. Acoust. Soc. Am. 115 (1) (2004) 146–156.
[11] H. Matt, I. Bartoli, F. Lanza di Scalea, Ultrasonic guided wave monitoring of composite wing skin-to-spar bonded joints in aerospace structures, J. Acoust. Soc. Am. 118 (2005) 2240–2252.
[12] G. Palardy, I. Fernandez Villegas, Ultrasonic welding of thermoplastic composites with flat energy directors: influence of the thickness of the energy director on the welding process, in: Proceedings of the 20th international conference on composite materials, Copenhagen, Denmark, 19–24 July 2015.
[13] A. Banatar, T.G. Gutowski, Ultrasonic welding of PEEK graphite APC-2 composites, Polym. Eng. Sci. 29 (23) (1989) 1705–1721.
[14] ASTM D1002–05, Standard Test Method for Apparent Shear Strength of Single-Lap-Joint Adhesively Bonded Metal Specimens by Tension Loading (Metal-to-Metal), October 2005.
[15] S. Daggumati, I. de Baere, W. van Paepegem, J. Degrieck, J. Xu, S.V. Lomov, I. Verpoest, Local damage in a 5-harness satin weave composite under static tension: part II - Meso-FE modelling, Compos. Sci. Technol. 70 (2010) 1934–1941.
[16] TenCate Cetex TC1100 PPS Resin System, TenCate Advanced Composites, Product Datasheet Revised 05/2014.
[17] V. Giurgiutiu, Tuned Lamb wave excitation and detection with piezoelectric wafer active sensors for structural health monitoring, J. Intell. Mater. Syst. Struct. 16 (2005) 291–305.
[18] C. Tong, B.L.N. Kennet, Automatic seismic event recognition and later phase identification for broadband seismograms, Bull. Seismol. Soc. Am. 86 (6) (1996) 1896–1909.
[19] D. Gagar, M. Martinez, M. Yanishevsky, B. Rocha, J. McFeat, P. Foote, P. Irving, Detecting and locating fatigue cracks in a complex wing-box structure using the acoustic emission technique: a verification study. in: Proceedings of the 9th International Workshop on SHM, Stanford, USA, 10–12 September 2013.
[20] N. Pérez, F. Buiochi, M.A.B. Andrade, J.C. Adamowski, Numerical characterization of soft piezoelectric ceramics, Int. Cong. Ultrason., AIP Conf. Proc. 1433 (2012) 648–651.
[21] V. Giurgiutiu, Structural health monitoring with piezoelectric wafer active sensors, second ed., Academic Press-Elsevier, San Diego, California, 2014.
[22] R. Courant, K. Friedrichs, H. Lewy, On the partial difference equations of mathematical physics, IBM J. Res. Dev. 11 (2) (1967) 215–234.
[23] J.H. Nieuwenhuis, J. Neumann, D.W. Greve, I.J. Oppenheim, Generation and detection of guided waves using PZT wafer transducers, IEEE Trans. Ultrason. Ferroelectr. Freq. Control 52 (11) (2005) 2103–2111.
[24] A.M. Zelenyak, M.A. Hamstad, M.G.R. Sause, Modeling of acoustic emission signal propagation in waveguides, Sensors 15 (2015) 11805–11822.
[25] P. Theobald, B. Zeqiri, J. Avison, Couplants and their influence on AE sensor sensitivity, J. Acoust. Emission 26 (2008) 91–97.
[26] P.D. Wilcox, Lamb wave inspection of large structures using permanently attached transducers, PhD Thesis, Imperial College London, 1998.

[27] SAE ARP6461, Guidelines for implementation of structural health monitoring on fixed wing aircraft, 2013.
[28] M. Dziendzikowski, A. Kurnyta, K. Dragan, S. Klysz, A. Leski, In situ barely visible impact damage detection and localization for composite structures using surface mounted and embedded PZT transducers: a comparative study, Mech. Syst. Signal Process. 78 (2016) 91–106.
[29] Z. Su, L. Ye, Identification of Damage Using Lamb Waves: From Fundamentals to Applications, in: F. Pfeiffer, P. Wriggers (Eds.), Lecture notes in applied and computational mechanics, vol. 48, Springer, 2009.